^{68}Ga-NOTA-Functionalized Ubiquicidin: Cytotoxicity, Biodistribution, Radiation Dosimetry, and First-in-Human PET/CT Imaging of Infections

Thomas Ebenhan[1], Mike M. Sathekge[1], Thabo Lengana[1], Michel Koole[2], Olivier Gheysens[2], Thavendran Govender[3], and Jan R. Zeevaart[4]

[1]Department of Nuclear Medicine, University of Pretoria and Steve Biko Academic Hospital, Pretoria, South Africa; [2]Nuclear Medicine and Molecular Imaging, University Hospitals Leuven, Leuven, Belgium; [3]Catalysis and Peptide Research Unit, University of KwaZulu-Natal, Durban, South Africa; and [4]Department of Science and Technology, Preclinical Drug Development Platform, North West University, Potchefstroom, South Africa

Ubiquicidin is an antimicrobial peptide with great potential for nuclear imaging of infectious diseases, as its cationic-rich fragment TGRAKRRMQYNRR (UBI) has been functionalized with NOTA to allow complexation to ^{68}Ga (^{68}Ga-NOTA-UBI). We herein assess the cytotoxicity and radiation dosimetry for ^{68}Ga-NOTA-UBI and a first-in-human evaluation to diagnose infectious processes. **Methods:** Cytotoxicity was evaluated in green monkey kidney epithelial (Vero) cells and MT-4 leukocytes. Tracer susceptibility was studied in vitro using different bacterial and fungal strains. PET/CT-based biodistribution, pharmacokinetics, and radiation dosimetry were performed on nonhuman primates. Two healthy volunteers and 3 patients with suspected infection underwent ^{68}Ga-NOTA-UBI PET/CT imaging. **Results:** Negligible cytotoxicity was determined for NOTA-UBI. ^{68}Ga-NOTA-UBI showed moderate blood clearance (29-min half-life) and predominant renal clearance in nonhuman primates. Human radiation dose estimates indicated the bladder wall as the dose-critical tissue (185 μSv/MBq), followed by the kidneys (23 μSv/MBq). The total absorbed body dose was low (<7 μSv/MBq); the effective dose was estimated at 17 μSv/MBq. ^{68}Ga-NOTA-UBI could diagnose bone- and soft-tissue infection in 3 of 3 patients. **Conclusion:** ^{68}Ga-NOTA-UBI is considered a nontoxic, safe-to-administer radiopharmaceutical unlikely to cause adverse effects in humans. The favorable tracer biodistribution and the first-in-human results will make ^{68}Ga-NOTA-UBI PET/CT an encouraging future diagnostic technique with auxiliary clinical relevance.

Key Words: ^{68}Ga; ubiquicidin; UBI29-41; PET/CT imaging; infection imaging; ^{68}Ga-NOTA-UBI(29-41)

J Nucl Med 2018; 59:334–339
DOI: 10.2967/jnumed.117.200048

Conventionally, bacterial infections are diagnosed by clinical examination, characteristic symptoms, and culturing of microorganisms from blood, urine, or sputum samples. Radiologic techniques such as ultrasound or CT may be helpful but cannot always differentiate septic from aseptic processes and identify only anatomic changes related to late-stage infections, whereas MRI cannot be applied to patients with claustrophobia or implanted medical devices.

Scintigraphy and PET can track radiolabeled leukocyte infiltration into the infection site using a whole-body imaging approach and allow for early detection of infectious areas well before anatomic changes occur (*1*). Approved radiopharmaceuticals to assess infectious diseases include in vitro or in vivo radiolabeled leukocytes, ^{18}F-FDG, ^{67}Ga-citrate, and radiolabeled antibodies targeting leukocyte antigens (*2*). However, the accuracy of these tracers in diagnosing infection varies considerably (*3*). Therefore, the development of bacteria-specific imaging probes is a promising alternative to more reliably detect infections (*4,5*). Radiolabeled antibiotics, vitamins, other biomimetics, antimicrobial peptides (AMPs), and bacteriophages have been highlighted as potential infection-imaging agents (*6–10*).

AMPs such as ubiquicidin are used as targeting vectors for molecular imaging because of their selectivity for bacterial cell membranes in the innate immune system response (*11*). Studies of cation-rich ubiquicidin fragments, including TGRAKRRMQYNRR (UBI) (*12*), have shown their usefulness as infection nuclear imaging agents. This peptide, directly labeled with ^{99m}Tc, shows preferential binding to bacterial rather than mammalian cells in vitro and allows identification of infected sites and better discrimination from the surrounding sterile or inflamed tissue in animals and human subjects (*13–15*). Although SPECT is a widely available technique, PET may be superior in terms of image resolution, sensitivity, and quantification. Therefore, a ^{68}Ga-radiolabeled PET derivative of UBI was developed, meeting the physiologic half-life of peptides (*16*) and using a biologic targeting vector (i.e., peptide bioconjugates). Chelation with the bifunctional chelator molecule NOTA (*17–19*) was used to conjugate UBI, allowing for ^{68}Ga radiolabeling (*20*). On radiosynthesis, a successful preclinical evaluation as a bacteria-selective imaging agent was approved in 3 different rabbit models (*21*). Before clinical application, the safety of radiopharmaceuticals regarding tolerability and possible side effects needs to be determined to a certain extent (*22*). We therefore aimed to demonstrate that ^{68}Ga-NOTA-UBI can be used as a safe radiopharmaceutical for human applications by achieving results regarding its in vitro cytotoxicity, biodistribution, and estimated human radiation dosimetry in nonhuman primates (NHPs). In addition, we report the results of a first-in-human study on the imaging performance of ^{68}Ga-NOTA-UBI PET/CT in patients with suspected infection.

Received Aug. 1, 2017; revision accepted Nov. 9, 2017.
For correspondence or reprints contact: Mike Sathekge, University of Pretoria and Steve Biko Academic Hospital, Private Bag X169, Pretoria 0001, South Africa.
E-mail: mike.sathekge@up.ac.za
Published online Oct. 19, 2017.

MATERIALS AND METHODS

This study was performed in accordance with the ethical standard of our institution and with the 1964 Helsinki Declaration and its later amendments. Informed consent was obtained from all patients.

Media, Chemicals, and Equipment

Solvents, drugs, and culture media were purchased from commercial sources in highest purity and used as recommended. NOTA-UBI was purchased from GL Biochem Ltd. To determine mammalian cell toxicity, an automated PowerWave XS2 microplate reader (Biotek Instruments) measuring optical density was utilized.

Bacteria, Fungi, and Laboratory Animals

Green monkey kidney epithelial (Vero) cells and MT-4 human leukocytes from LGC Standards were used to assess in vitro cytotoxicity. Bacterial cells (*Escherichia coli* [ATCC 25922], *Staphylococcus aureus* [ATCC 25923], *Pseudomonas aeruginosa* [ATCC 27853], and *Bacillus subtilis* [ATCC 6051]) and fungi (*Candida albicans* [ATCC 24433], *C. albicans* [ATCC 90028], and *Candida parasilopsis* [ATCC 22019]) were obtained from National Health Laboratory Services.

$^{nat/68}$Ga-Labeling of NOTA-UBI

NOTA-functionalized UBI was labeled cold with gallium(III)chloride ($^{nat}GaCl_3$) (for in vitro assays) or radiolabeled with generator-derived $^{68}Ga[Cl_4]^-$ (all in vivo applications) as described previously (*20*).

Cytotoxicity

Vero cells were used studying any noxious potential of NOTA, NOTA-UBI, and ^{nat}Ga-NOTA-UBI as previously described (*23*). Additionally, cytotoxicity to MT-4 leukocytes was determined by compound dose escalation or calculating the half-maximal inhibitory concentration (IC_{50}) (*24*).

Antibacterial and Antifungal Susceptibility

Bacterial susceptibility was determined using the broth microdilution method (*25*) on freshly cultured bacterial strains with a final working suspension of 10^6 cells/mL. The fungal susceptibility was evaluated in yeast strains by a method described elsewhere (*26*) using a working suspension of 5×10^3 cells/mL.

^{68}Ga-NOTA-UBI Pharmacokinetics and Tracer Biodistribution in NHPs

The study enrolled three adult vervet monkeys (NHPs) according to the South African code of practice for the care and use of animals. Ethical approval was given by the Pretoria University (H001-09). The Biomedical Research Centre (Onderstepoort, Pretoria University) provided and handled the NHPs as previously described (*27*).

Dosimetric Analyses in NHPs

Absorbed radiation doses were calculated according to the MIRD method (OLINDA/EXM 1.0) for internal dose assessment (*28*).

PET/CT Imaging in Humans

Two healthy volunteers and three patients with known or suspected infection were approved for this first-in-human study by the institutional Ethics Committee. The first patient was a 37-year-old man with unilateral ankle joint infection and osteomyelitis suggested on prior bone scintigraphy. The second was a 34-year-old woman diagnosed with septic ankle osteomyelitis on the basis of ^{99m}Tc-WBC scintigraphy. The third was a 69-year-old woman with a history of diskitis who presented with worsening pain and increased inflammatory parameters.

Whenever possible, blood cultures and bacteriology were performed, confirming the infection. The results of clinical tests, radiography, and bone scintigraphy were used when tissue samples could not be cultured. Nuclear imaging was performed using a previously published procedure (*27*).

Statistical Analyses

Results were expressed as mean ± SD or as SE of mean ± SEM. When indicated, representative data from individual experiments are shown. Statistical significance was determined using the Student *t*-test. A P value of < 0.05 was considered statistically significant.

RESULTS

Cytotoxicity

Cytotoxicity was tested by escalating compound concentrations in Vero cells (Supplemental Fig. 1; supplemental materials are available at http://jnm.snmjournals.org) and by standard IC_{50} calculations in MT-4 leukocytes. Vero cells sustained cellular viability on the maximum treatment concentration of 200 μM ($P > 0.05$). The percentage of viable cells was calculated as 97.7 ± 4.1, 98.1 ± 2.1, 95.8 ± 3.7, 90.8 ± 8.3, and 96.6 ± 3.7 for UBI, NOTA-UBI, ^{nat}Ga-NOTA-UBI, ^{nat}Ga-NOTA, and the control, respectively. A significant cytotoxic response was found with 0.1–4 ppm of $CdCl_2$ (positive control); the percentage of viable cells seemingly decreased with increasing $CdCl_2$ amounts ($r^2 = 0.85$), with significant differences in comparison to all tested compounds ($P < 0.01$). Leukocytes exhibited no cytotoxicity; the IC_{50} values (mM) were 340, 270, and 260 for UBI, NOTA-UBI, and ^{nat}Ga-NOTA-UBI, respectively. No leukocyte toxicity occurred on treatment with indinavir (control, $IC_{50} = 301$ nM).

Antimicrobial and Antifungal Susceptibility

The tested UBI derivatives exhibited no substantial antibacterial or antifungal activity and caused insignificant inhibition of bacterial or fungal growth up to a maximum concentration (0.2 mg/mL), being 10,000-fold higher than the tracer concentration considered in human blood. In the same assay, the minimal inhibitory concentrations (μg/mL) of neomycin were 0.32, 0.87, 2.0, and 32.6 for *S. aureus, B. subtilis, E. coli,* and *P. aeruginosa,* respectively. The minimal inhibitory concentrations (μg/mL) determined for clotrimazole were 0.04, 0.03, and 1.0 for *C. albicans* 24433, *C. albicans* 90028, and *C. parasilopsis,* respectively.

^{68}Ga-NOTA-UBI Imaging, Pharmacokinetics, and Biodistribution in NHPs

NHPs received a 33–45 MBq/kg dose of ^{68}Ga-NOTA-UBI (244 ± 50 MBq; specific activity, 13.8 ± 1.9 GBq/μmol). A 3.5- to 6.5-mL saline bolus contained 29.7 ± 2.1 nmol of NOTA-UBI (distributed as 72 ± 19 pmol/mL of blood) (Supplemental Table 1). Maximum-intensity projection PET/CT showed early-onset tracer biodistribution, with the highest tracer concentrations in the bladder, kidneys, liver, and heart (Fig. 1). Significant tracer washout over 120 min was determined for blood, heart, spleen, lung, stomach, thyroid, bone, genitals, and muscle. The SUVs of all other organs were similar or lower than those of musculoskeletal tissue (Supplemental Table 2). The time–activity curves resulting from blood and urine sampling illustrated relatively rapid tracer blood clearance (2.64 percentage injected dose [%ID]/h) (Supplemental Fig. 2) following an exponential function (29-min half-life, $r^2 = 0.77$; $n = 19$; peak concentration, 0.49 ± 0.19 %ID/g). Radioactivity was recovered predominately via the renal excretion route as follows: 15.4 %ID/h excretion rate, 74 ± 4 %ID cumulative percentage recovery voiding over 120 min, and a peak concentration of 39 ± 8 %ID ($r^2 = 0.90$; $n = 17$).

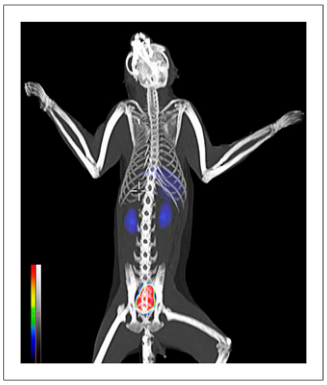

FIGURE 1. Representative ^{68}Ga-NOTA-UBI PET/CT biodistribution in NHPs 60 min after tracer administration (189 MBq).

Estimation of Human Absorbed Doses by Extrapolating Data from ^{68}Ga-NOTA-UBI Biodistribution in NHPs

Human radiation doses represent the organ-related burden to a normal-sized adult. The extrapolated tracer biodistribution in humans based on ^{68}Ga-NOTA-UBI injection into NHPs is summarized in Supplemental Table 3. Absorbed doses (Table 1) were calculated from integrated organ residence times (Supplemental Table 4). The effective dose was 17 ± 6 μSv/MBq, estimating a total human dose range of between 3.1 and 4.3 mSv/tracer administration. Because of the dominantly renal excretion route, the radioactive burden was the highest in the bladder wall and kidneys. Secondary critical organs were liver and lung. All other values were no more than 10 μSv/MBq. A low total-body dose of less than 7 μSv/MBq was absorbed.

TABLE 1
Extrapolated Human Radiation Dose Estimates for ^{68}Ga-NOTA-UBI

Organ	Dose (μSv/MBq)	%CV
Adrenals	6.21	5.0
Brain	1.16	9.5
Breast	4.95	7.4
Gallbladder wall	6.84	5.5
Lower left intestine	8.50	15.5
Small intestine	7.58	7.0
Stomach wall	6.56	2.4
Upper left intestine	7.28	6.9
Heart wall	10.00	6.8
Kidneys	23.10	19.0
Liver	17.70	27.9
Lung	11.70	13.3
Muscle	3.70	9.7
Ovaries	7.60	10.0
Pancreas	6.15	21.0
Red marrow	6.67	5.6
Osteogenic cells	9.64	5.8
Skin	4.59	5.2
Spleen	7.67	15.5
Testes	5.01	25.6
Thymus	5.35	6.7
Thyroid	3.55	4.5
Urinary bladder wall	185.00	58.6
Uterus	10.30	22.2
Total body	6.84	0.6

%CV = coefficient of variance (%).

PET/CT Imaging in Humans

Two 18-y-old healthy volunteers (1 man and 1 woman) and 3 patients (1 man and 2 women; age range, 34–69 y) with known or suspected bone- or soft-tissue infections received 174 ± 42 MBq (range, 129–240 MBq) of ^{68}Ga-NOTA-UBI, corresponding to 22.5 ± 3.8 nmol (range, 21.3–25.5 nmol) of NOTA-UBI (Supplemental Table 1). The patients had no acute adverse reactions such as altered blood pressure, rash, itching, flushing, nausea, coughing, muscle cramps, or dizziness on tracer injection (no long-term adverse effects were reported either). The PET images of the healthy volunteers showed tracer accumulation in the kidneys and bladder, representing renal excretion (Fig. 2). Minimal radioactivity was noted in the liver and myocardium (including vasculature system). The respective tracer concentrations (n = 5; SUV_{mean} ± SD) for the heart, lung, liver, spleen, kidneys, urinary bladder, and muscle tissue were 2.28 ± 0.4, 0.57 ± 0.1, 1.78 ± 0.8, 1.37 ± 0.5, 11.03 ± 7.6, 20.88 ± 5.9, and 0.32 ± 0.1. In 3 of 3 patients (100%), ^{68}Ga-NOTA-UBI PET/CT accurately identified the infectious areas that have also been confirmed by other techniques. All ^{68}Ga-NOTA-UBI PET images showed a significantly higher SUV at the infection site than in reference tissues ($P < 0.05$) resulting in high target-to-background ratios and good delineation of the infectious regions. Images of a representative patient with chronic osteomyelitis in the ankle joint with extending soft-tissue infection into the legs, confirmed by radiography and bone scintigraphy, are shown in Figure 3. Figure 4 shows a spinal infection in a 69-y-old patient, which was confirmed by MRI and further clinical testing. The SUV_{max} at the infection site was 3.3 ± 0.3, and the SUV_{mean} was 3.1–3.6-fold higher in infected tissue than in noninfected tissue ($P < 0.001$).

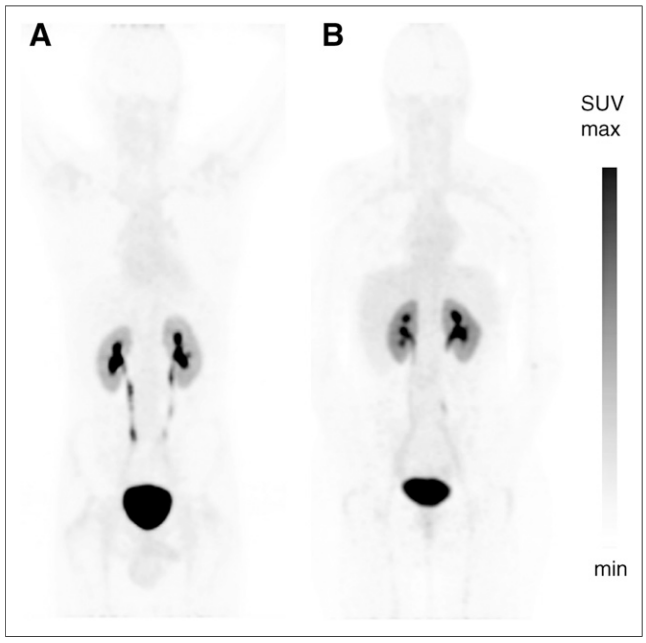

FIGURE 2. ^{68}Ga-NOTA-UBI PET maximum-intensity projection (skull to midthigh) demonstrating physiologic tracer biodistribution in healthy male (A) and female (B) volunteers. Images were acquired 60 min after intravenous injection of 129 and 132 MBq, respectively, of tracer.

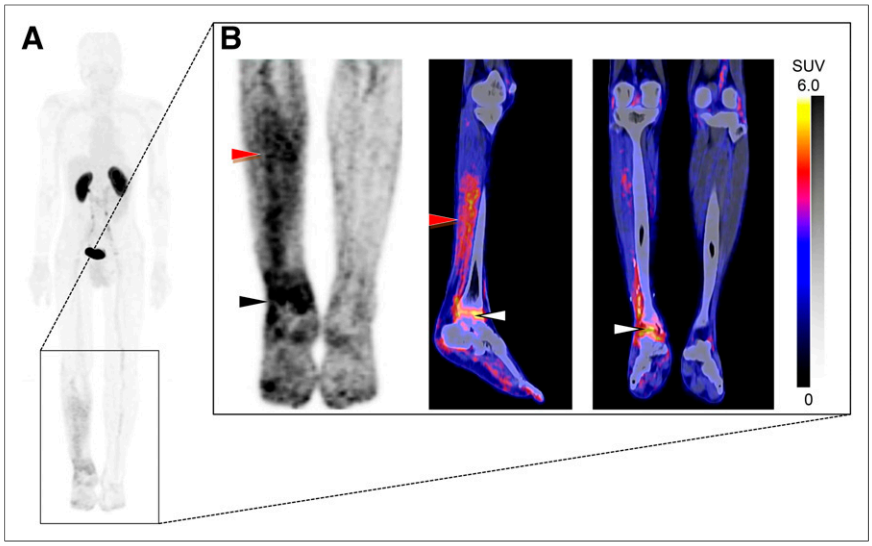

FIGURE 3. ^{68}Ga-NOTA-UBI PET/CT images in representative patient with peripheral bone- and soft-tissue infection. (A) Whole-body maximum-intensity projection shows diffusely increased tracer uptake in right lower leg. (B) Detailed images demonstrate focal increased tracer uptake in ankle joint extending to adjacent bone (black and white arrows), as well as diffuse tracer uptake in calf muscles (red arrows); no significant uptake in contralateral leg was noted. Images were obtained 60 min after tracer administration (240 MBq).

DISCUSSION

Novel approaches have been proposed and performed to conquer the challenges in imaging infectious diseases, including discriminating infection from sterile inflammation, tracking the spread of infection, and monitoring therapy (*5,29*). It is known that slight modifications of a molecule may significantly alter its biologic properties, hence necessitating evaluation of any tracer derivative to determine its efficacy and safety before human administration (*30,31*).

Toxicity

Our cellular testing showed minimal toxicity to cultured Vero cells, suggesting negligible toxicity to patients. The antimicrobial activity against selected bacterial and fungal strains showed minimal toxicity, as is expected since toxicity would be counterproductive for AMPs. These strains are naturally found in humans and other mammals and never exhibit significant toxicity toward the organism's host cells (*7,32,33*). The lack of antimicrobial activity is advantageous for this diagnostic agent because killing of the targeted bacteria could result in trafficking of dead pathogens and the attached tracer to remote sites, thereby distorting the image and interpretation as to the extent of the infectious focus (*32,34*). The observed lack of antimicrobial activity was in contradiction to the results of Brouwer et al. (*22*). UBI has been reported to exhibit noteworthy toxicity against methicillin-resistant *S. aureus*; however, a non–methicillin-resistant, staphylococcal strain and different methods were used here. AMP susceptibility to methicillin-resistant *S. aureus* was also proven for other peptides (*35*). Despite the lack of susceptibility, an uncompromised bacterial binding affinity was reported for ^{68}Ga-NOTA-UBI (*6,20,36*). Lupetti et al. (*37*) studied the antifungal activity of UBI against *Aspergillus fumigates* hyphae and reported an IC_{50} of 0.15 ± 0.03 mg/mL. Although the fungi species was different, antifungal activity against *Aspergillus fumigates* and *Candida* species was minimal. As with antibacterial activity, antifungal activity is not required, but unabridged binding affinity is desired for radiodiagnostic agents to facilitate infection imaging.

^{68}Ga-NOTA-UBI Imaging and Dosimetry

Because UBI, as an AMP, was expected to be nonimmunogenic and was considered nontoxic, its evaluation for scintigraphic imaging was initially fast-tracked (*38*). ^{99m}Tc-UBI29-41 was administered to humans to study pharmacokinetics after tracer injection in vivo (*39*). Thereafter, a first-in-human study enrolled patients with infection of bone, soft tissue, or prostheses. No adverse effects occurred after ^{99m}Tc-UBI29-41 imaging of the infectious scenarios (*14*). Recently, we have shown that NOTA conjugation of UBI29-41 did not compromise the ability of this AMP fragment to selectively bind to the bacterial cell envelope (*20*). Presently, no published study has focused on the safe administration of ^{68}Ga-NOTA-UBI and its translation into clinical applications. We generated initial findings during a proof-of principle investigation in which ^{68}Ga-NOTA-UBI was safely administered to rabbits bearing muscular infection paired with a contralateral sterile inflammation site (*21*). Similar results from another research group support our findings using infected mice. The tracer was found to be stable in phosphate-buffered saline and blood samples (*37,40*). All animals tolerated the tracer injections well; it seems safe to predict a negligible risk concerning the administration of ^{68}Ga-NOTA-UBI.

Here, we have demonstrated radiation dosimetry estimates in NHPs translatable to human applications of ^{68}Ga-NOTA-UBI. These results should be considered preliminary, as they are based on a setup with 3 male subjects undergoing ^{68}Ga-NOTA-UBI

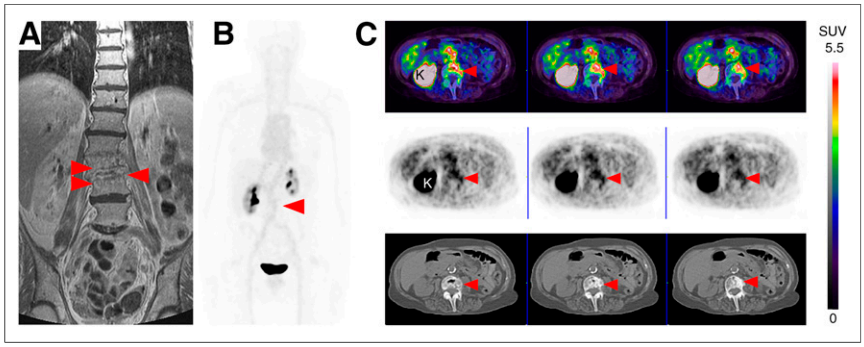

FIGURE 4. Representative MR and ^{68}Ga-NOTA-UBI PET/CT images in patient with suspected spinal infection (spondylodiskitis). (A–C) Coronal T1-weighted MR image (fat suppression) (A), whole-body maximum-intensity-projection PET image (B), and sequential transaxial fused PET/CT (top), PET (middle), and CT (bottom) images (C) showing focally increased uptake (arrowheads) in intervertebral region of L3–L4 corresponding to abnormal findings on MRI. K = kidney.

PET/CT to study blood clearance, tissue biodistribution, tracer excretion, and estimation of radiation doses. The vervet monkey biomedical model is reported to suit several investigations such as behaviorism, metabolism, and immunity (*41*). The similarity in blood distribution volume between this model and humans (60–70 mL/kg) has significantly stimulated use of the model to translate advanced radiopharmaceuticals to humans. The bolus injection, activity concentration, specific activity, and total peptide mass injected in NHPs mimicked those considered for human application, yet the lower animal body weight increased the injected dose by 15-fold as compared with human doses. The study design included simple access to blood and urine samples, which allowed statistical compliance in a small number of animals, compared with rodents. A desirable ^{68}Ga-NOTA-UBI blood clearance over 60–90 min was determined ($P < 0.001$). On the basis of this result, the first-in-human investigations presented here were set for static imaging at 60 min after tracer injection. The lack of hepatobiliary tracer excretion is favorable and may suggest the feasibility of ^{68}Ga-NOTA-UBI PET for diagnosis of abdominal infection. The overall radiation dose and the dose to regenerative tissues such as red marrow, osteogenic cells, ovaries, and gonads were favorably low (<10 μSv/MBq). Only male monkeys were studied, however; radiation dose estimates for ovaries, uterus, and breasts relied on the assumption that the tracer biodistribution is similar for women and men. The bladder was voided to create urine samples and to mimic the clinical setup in which the patients void the bladder ahead of imaging. The human dose range was calculated as 3.1–4.3 mSv per ^{68}Ga-NOTA-UBI administration, which adheres to the European guidelines on maximum exposure for a single radioactive injection (10 mSv) (*42*). No comparative dosimetry of other ^{68}Ga-labeled infection-imaging agents is currently available. The radiation for one ^{68}Ga-NOTA-UBI dose is significantly lower than for ^{18}F-FDG ($P < 0.05$) and 3.5 times less than for ^{68}Ga-DOTATATE, another diagnostic ^{68}Ga tracer used in humans (*43,44*).

PET/CT Imaging in Humans

This first-in-human study evaluating the diagnostic performance of ^{68}Ga-NOTA-UBI PET/CT was performed on 3 patients with known or suspected bone- or soft-tissue infection. Except for the renal clearance and excretion, biodistribution in humans was similar to that in NHPs, and no significant differences were observed between healthy volunteers and patients except for tracer accumulation in the infectious area. The accumulation of ^{68}Ga-NOTA-UBI over 60 min was sufficient to delineate the infectious tissues, as shown by a target-to-nontarget ratio of 3.4 ± 0.2, which is significantly higher ($P < 0.05$) than the reported values for ^{99m}Tc-UBI29-41 (2.3 ± 1.3; $n = 18$) or ^{99m}Tc-HYNIC-UBI29-41 (1.9 ± 0.3; $n = 5$) (*14,45*). Our pilot study demonstrated the ability of this imaging technique to detect infected tissues as confirmed by other techniques. Tracer uptake based on this targeting approach is reflected by the bacterial burden rather than by the inflammatory cell influx as observed with PET imaging using ^{18}F-FDG or radiolabeled leukocytes. We described previously that NOTA-UBI uptake follows an exponential dependence ($R^2 > 0.66$) with rising amounts of bacteria (gram-positive or -negative) residing in the infection site (*46*). Like NOTA-UBI, the novel bacteria-specific PET probe 2-fluoro-^{18}F-desoxysorbitol was developed in mice, was tested recently on healthy volunteers, and is expected to diagnose Enterobacteriaceae-specific infection in humans (*47,48*). The host-independent targeting mechanism of UBI could qualify ^{68}Ga-NOTA-UBI PET/CT as an imaging modality to facilitate future differential diagnosis of infectious diseases.

Study Scope and Limitations

Some limitations of this study included the fact that tracer pharmacokinetics, biodistribution, and dosimetry data were obtained from anesthetized NHPs, which could affect the hemodynamics of various organs and may affect tracer uptake. Although the blood flow to the liver is altered less by isoflurane than by other anesthesia methods, renal blood flow and urine production are decreased by isoflurane in mice (*49*). General anesthesia could also affect the metabolism of ^{68}Ga-NOTA-UBI, similarly to the significant reduction in brain glucose metabolism observed with ^{18}F-FDG (*50*). This study allowed for only 3 male NHPs, thus limiting its statistical power and assumptive information on radiation burden in females. Because of the avid urinary tracer excretion, imaging of infections in the urinary tract or pelvis may be inferior. However, more favorable renal excretion was seen in human subjects than in NHPs. Also, diuretic administration, bladder voiding, or catheterization can significantly lower the dose to the bladder wall. Even though there is a major advantage to using radiolabeled AMPs (they are retained at the site of infection by internalization and subsequent amplification), imaging of phagocytosed microorganisms may be limited (*13*), potentially underestimating the actual bacterial burden.

CONCLUSION

This study demonstrated that ^{68}Ga-NOTA-UBI is a nontoxic, safe-to-administer radiopharmaceutical unlikely to cause adverse effects in humans. Biodistribution corresponds to major peptide-metabolizing organs and predominantly urinary excretion. ^{68}Ga-NOTA-UBI PET/CT could accurately identify all infectious foci in 3 patients with suspected infection. Even though the first-in-human results are encouraging, further clinical studies are required to assess the diagnostic accuracy of ^{68}Ga-NOTA-UBI for imaging infectious diseases.

DISCLOSURE

Financial support was given by the DST via the Nuclear Technologies in Medicine and the Biosciences Initiative, which is managed by Necsa. No other potential conflict of interest relevant to this article was reported.

ACKNOWLEDGMENTS

We thank Dr. Raveen Parboosing for contributing to all cellular assays, Prof. Vinny Naidoo and Dr. Tamsyn Pulker for NHP surveillance, Dr. Moshe Modiselle for recruiting the healthy volunteers and patients, and Mrs. Delene van Wyk for assisting with image acquisition.

REFERENCES

1. Goldsmith SJ, Vallabhajosula S. Clinically proven radiopharmaceuticals for infection imaging: mechanisms and applications. *Semin Nucl Med.* 2009;39:2–10.
2. Boerman OC, Dams ET, Oyen WJ, Corstens FH, Storm G. Radiopharmaceuticals for scintigraphic imaging of infection and inflammation. *Inflamm Res.* 2001;50:55–64.
3. Sathekge M, Maes A, D'Asseler Y, Vorster M, Van de Wiele C. Nuclear medicine imaging in tuberculosis using commercially available radiopharmaceuticals. *Nucl Med Commun.* 2012;33:581–590.
4. Signore A, D'Alessandria C, Lazzeri E, Dierckx R. Can we produce an image of bacteria with radiopharmaceuticals? *Eur J Nucl Med Mol Imaging.* 2008;35:1051–1055.
5. Bunschoten A, Welling MM, Termaat MF, Sathekge M, van Leeuwen FW. Development and prospects of dedicated tracers for the molecular imaging of bacterial infections. *Bioconjug Chem.* 2013;24:1971–1989.

6. Signore A, Chianelli M, D'Alessandria C, Annovazzi A. Receptor targeting agents for imaging inflammation/infection: where are we now? *Q J Nucl Med Mol Imaging.* 2006;50:236–242.
7. Lupetti A, Nibbering PH, Welling MM, Pauwels EK. Radiopharmaceuticals: new antimicrobial agents. *Trends Biotechnol.* 2003;21:70–73.
8. Basu S, Chryssikos T, Moghadam-Kia S, Zhuang H, Torigian DA, Alavi A. Positron emission tomography as a diagnostic tool in infection: present role and future possibilities. *Semin Nucl Med.* 2009;39:36–51.
9. Kumar V, Boddeti DK. ^{68}Ga-radiopharmaceuticals for PET imaging of infection and inflammation. *Recent Results Cancer Res.* 2013;194:189–219.
10. Sathekge M. The potential role of ^{68}Ga-labeled peptides in PET imaging of infection. *Nucl Med Commun.* 2008;29:663–665.
11. Ebenhan T, Gheysens O, Kruger HG, Zeevaart JR, Sathekge MM. Antimicrobial peptides: their role as infection-selective tracers for molecular imaging. *BioMed Res Int.* 2014;2014:867381.
12. Hiemstra PS, van den Barselaar MT, Roest M, Nibbering PH, van Furth R. Ubiquicidin, a novel murine microbicidal protein present in the cytosolic fraction of macrophages. *J Leukoc Biol.* 1999;66:423–428.
13. Nibbering PH, Welling MM, Paulusma-Annema A, Brouwer CP, Lupetti A, Pauwels EK. ^{99m}Tc-labeled UBI29-41 peptide for monitoring the efficacy of antibacterial agents in mice infected with Staphylococcus aureus. *J Nucl Med.* 2004;45:321–326.
14. Akhtar MS, Qaisar A, Irfanullah J, et al. Antimicrobial peptide ^{99m}Tc-ubiquicidin 29-41 as human infection-imaging agent: clinical trial. *J Nucl Med.* 2005;46:567–573.
15. Brouwer CP, Sarda-Mantel L, Meulemans A, Le Guludec D, Welling MM. The use of technetium-99m radiolabeled human antimicrobial peptides for infection specific imaging. *Mini Rev Med Chem.* 2008;8:1039–1052.
16. Fani M, Andre JP, Maecke HR. ^{68}Ga-PET: a powerful generator-based alternative to cyclotron-based PET radiopharmaceuticals. *Contrast Media Mol Imaging.* 2008;3:67–77.
17. Velikyan I, Beyer GJ, Bergström-Pettermann E, Johansen P, Bergström M, Långström B. The importance of high specific radioactivity in the performance of ^{68}Ga-labeled peptide. *Nucl Med Biol.* 2008;35:529–536.
18. Velikyan I. Prospective of ^{68}Ga-radiopharmaceutical development. *Theranostics.* 2013;4:47–80.
19. Velikyan I. Positron emitting [^{68}Ga]Ga-based imaging agents: chemistry and diversity. *Med Chem.* 2011;7:345–379.
20. Ebenhan T, Chadwick N, Sathekge MM, et al. Peptide synthesis, characterization and ^{68}Ga-radiolabeling of NOTA-conjugated ubiquicidin fragments for prospective infection imaging with PET/CT. *Nucl Med Biol.* 2014;41:390–400.
21. Ebenhan T, Zeevaart JR, Venter JD, et al. Preclinical evaluation of ^{68}Ga-labeled 1,4,7-triazacyclononane-1,4,7-triacetic acid-ubiquicidin as a radioligand for PET infection imaging. *J Nucl Med.* 2014;55:308–314.
22. Brouwer CP, Bogaards SJ, Wulferink M, Velders MP, Welling MM. Synthetic peptides derived from human antimicrobial peptide ubiquicidin accumulate at sites of infections and eradicate (multi-drug resistant) *Staphylococcus aureus* in mice. *Peptides.* 2006;27:2585–2591.
23. Pawar SA, Jabgunde AM, Govender P, et al. Synthesis and molecular modelling studies of novel carbapeptide analogs for inhibition of HIV-1 protease. *Eur J Med Chem.* 2012;53:13–21.
24. Mokaleng BB, Ebenhan T, Ramesh S, et al. Synthesis, ^{68}Ga-radiolabeling and preliminary in vivo assessment of a depsipeptide-derived compound as a potential PET/CT infection imaging agent. *BioMed Res Int.* 2015;2015:284354.
25. Eloff JN. A sensitive and quick microplate method to determine the minimal inhibitory concentration of plant extracts for bacteria. *Planta Med.* 1998;64:711–713.
26. Cuesta I, Bielza C, Larranaga P, et al. Evaluation by data mining techniques of fluconazole breakpoints established by European Committee on Antimicrobial Susceptibility Testing. *Antimicrob Agents Chemother.* 2009;53:2949–2954.
27. Ebenhan T, Schoeman I, Rossouw DD, et al. Evaluation of a flexible NOTA-RGD kit solution using gallium-68 from different ^{68}Ge/^{68}Ga-generators: pharmacokinetics and biodistribution in nonhuman primates and demonstration of solitary pulmonary nodule imaging in humans. *Mol Imaging Biol.* 2017;19:469–482.
28. Stabin MG, Sparks RB, Crowe E. OLINDA/EXM: the second-generation personal computer software for internal dose assessment in nuclear medicine. *J Nucl Med.* 2005;46:1023–1027.
29. Palestro CJ. Radionuclide imaging of osteomyelitis. *Semin Nucl Med.* 2015; 45:32–46.
30. Blok D, Feitsma RI, Vermeij P, Pauwels EJ. Peptide radiopharmaceuticals in nuclear medicine. *Eur J Nucl Med.* 1999;26:1511–1519.
31. Rennen HJ, Corstens FH, Oyen WJ, Boerman OC. New concepts in infection/inflammation imaging. *Q J Nucl Med.* 2001;45:167–173.
32. Brouwer CP, Wulferink M, Welling MM. The pharmacology of radiolabeled cationic antimicrobial peptides. *J Pharm Sci.* 2008;97:1633–1651.
33. Guaní-Guerra E, Santos-Mendoza T, Lugo-Reyes SO, Teran LM. Antimicrobial peptides: general overview and clinical implications in human health and disease. *Clin Immunol.* 2010;135:1–11.
34. Welling MM, Hiemstra PS, van den Barselaar MT, et al. Antibacterial activity of human neutrophil defensins in experimental infections in mice is accompanied by increased leukocyte accumulation. *J Clin Invest.* 1998;102:1583–1590.
35. Welling MM, Brouwer CP, van 't Hof W, Veerman EC, Amerongen AV. Histatin-derived monomeric and dimeric synthetic peptides show strong bactericidal activity towards multidrug-resistant Staphylococcus aureus in vivo. *Antimicrob Agents Chemother.* 2007;51:3416–3419.
36. Vilche M, Reyes AL, Vasilskis E, Oliver P, Balter H, Engler H. ^{68}Ga-NOTA-UBI-29-41 as a PET tracer for detection of bacterial infection. *J Nucl Med.* 2016;57:622–627.
37. Lupetti A, van Dissel JT, Brouwer CP, Nibbering PH. Human antimicrobial peptides' antifungal activity against Aspergillus fumigatus. *Eur J Clin Microbiol Infect Dis.* 2008;27:1125–1129.
38. Ferro-Flores G, Arteaga de Murphy C, Pedraza-Lopez M, et al. In vitro and in vivo assessment of ^{99m}Tc-UBI specificity for bacteria. *Nucl Med Biol.* 2003; 30:597–603.
39. Meléndez-Alafort L, Rodriguez-Cortes J, Ferro-Flores G, et al. Biokinetics of ^{99m}Tc-UBI 29-41 in humans. *Nucl Med Biol.* 2004;31:373–379.
40. Bhatt J, Mukherjee A, Korde A, Kumar M, Sarma HD, Dash A. Radiolabeling and preliminary evaluation of Ga-68 labeled NODAGA-ubiquicidin fragments for prospective infection imaging. *Mol Imaging Biol.* 2017;19:59–67.
41. Jasinska AJ, Schmitt CA, Service SK, et al. Systems biology of the vervet monkey. *ILAR J.* 2013;54:122–143.
42. Verbruggen A, Coenen HH, Deverre JR, et al. Guideline to regulations for radiopharmaceuticals in early phase clinical trials in the EU. *Eur J Nucl Med Mol Imaging.* 2008;35:2144–2151.
43. Hartmann H, Freudenberg R, Oehme L, et al. Dosimetric measurements of ^{68}Ga-high affinity DOTATATE: twins in spirit—part III. *Nuklearmedizin.* 2014;53: 211–216.
44. Deloar HM, Fujiwara T, Shidahara M, Nakamura T, Yamadera A, Itoh M. Internal absorbed dose estimation by a TLD method for ^{18}F-FDG and comparison with the dose estimates from whole body PET. *Phys Med Biol.* 1999;44:595–606.
45. Gandomkar M, Najafi R, Shafiei M, et al. Clinical evaluation of antimicrobial peptide [^{99m}Tc/Tricine/HYNIC^{0}]ubiquicidin 29-41 as a human-specific infection imaging agent. *Nucl Med Biol.* 2009;36:199–205.
46. Ebenhan T, Venter JD, Maguire GEM, et al. Novel radiopharmaceutical and preclinical aspects of Ga-68-UBI: a selective PET tracer for imaging of infection [abstract]. *J Nucl Med.* 2015;56(suppl 2):2A–30.
47. Zhu W, Yao S, Xing H, et al. Biodistribution and radiation dosimetry of the Enterobacteriaceae-specific imaging probe [^{18}F]fluorodeoxysorbitol determined by PET/CT in healthy human volunteers. *Mol Imaging Biol.* 2016;18:782–787.
48. Weinstein EA, Ordonez AA, Demarco VP, et al. Imaging Enterobacteriaceae infection in vivo with ^{18}F-fluorodeoxysorbitol positron emission tomography. *Sci Transl Med.* 2014;6:259ra146.
49. Fueger BJ, Czernin J, Hildebrandt I, et al. Impact of animal handling on the results of ^{18}F-FDG PET studies in mice. *J Nucl Med.* 2006;47:999–1006.
50. Alstrup AK, Smith DF. Anaesthesia for positron emission tomography scanning of animal brains. *Lab Anim.* 2013;47:12–18.